

Impact of random nanoscale roughness on gas-scattering dynamicsYichong Chen ^{*}, Livio Gibelli [†], and Matthew K. Borg *Institute for Multiscale Thermo fluids, School of Engineering, University of Edinburgh EH9 3FB, United Kingdom*

(Received 26 January 2024; accepted 5 June 2024; published 20 June 2024)

The impact of nanoscale wall roughness on rarefied gas transport is widely acknowledged, yet the associated scattering dynamics largely remain elusive. In this paper, we develop a scattering kernel for surfaces having nanoscale roughness that distinctly characterizes the two major types of interactions between gas molecules and rough surfaces. Namely these are (a) the weak perturbations arising from the thermal motion of wall atoms, essentially gas-phonon collisions, which are captured by the well-established Cercignani-Lampis model, and (b) the hard collisions owing to the irregularities of the rough, static potential energy surface, which are generally described by the fully diffuse model. Drawing an analogy between wave-surface and gas-surface scattering, a pseudo Debye-Waller factor is incorporated into the modeling as a weighting coefficient to allow the transition between smooth and rough surface conditions. The proposed scattering kernel is validated through high-fidelity molecular dynamics simulations that are performed for systems with varying roughness, temperature, and gas-surface combinations. The results indicate that the model well captures the scattering dynamics of gas molecular beams impinging on surfaces at different velocities, specifically for the accommodation coefficients and reflection patterns. Additionally, in flow and heat transport cases, it accurately predicts macroscopic quantities such as velocity slip and temperature jumps across the range of tested conditions.

DOI: [10.1103/PhysRevE.109.065308](https://doi.org/10.1103/PhysRevE.109.065308)**I. INTRODUCTION**

Engineering fluid systems operating at low pressures or micro- or nanoscales often indicate the breakdown of local quasithermodynamic equilibrium, necessitating a different modeling approach that goes beyond standard continuum fluid dynamics. In these problems, the fluid behavior must then be modelled using the Boltzmann or a kinetic model equation, supplemented by boundary conditions that model gas-surface interactions (GSIs). As gas rarefaction increases, gas molecules increasingly collide with wall atoms, making GSIs critical in simulating nonequilibrium gas dynamics. These interactions, which are molecular in nature, determine the velocity slip and temperature jump at the surface, which are macroscopic manifestations of fluid nonequilibrium conditions and significantly influence the overall flow field.

GSIs are conventionally formulated through scattering kernels (SKs) [1–13], establishing a probabilistic connection between incident and reflected molecular flux at the surface. These SKs generally include adjustable parameters known as accommodation coefficients (ACs) [6,14], which describe how physical properties of the impinging molecular flux (e.g. momentum and energy) are accommodated to the state

of the surface. Physically grounded representations of GSIs have also been considered, either by simplifying them to consider only binary collisions between gas molecules and effective surface cubes [15–18] or, more comprehensively, by solving kinetic equations within a very thin layer near the surface, modeling the behavior of gas molecules subjected to a static potential field from fixed wall atoms and colliding with phonons representing the fluctuating surface potential [19–27].

While substantial efforts have been invested in providing more accurate descriptions of GSIs, the role of nanoscale surface roughness has been notably under-represented [23]. Conventional SKs tend to model surface roughness by simply tweaking ACs, without relating them to the detailed scattering dynamics. Although pioneering experimental studies [28–32] and subsequent numerical research [33–35] demonstrate variations in the ACs of gases on rough surfaces compared to their smooth (polished) counterparts, the relationship between ACs and roughness is not always fully understood, as discussed in a recent work [36]. Furthermore, ACs alone are inadequate to capture the effects of roughness on gas-scattering dynamics. This can be seen from numerical studies using the same ACs in various SKs, but producing different macroscopic properties [10,37,38], and experiments where ACs are extracted based on pre-assumed SKs [39,40]. Therefore, the relationship between ACs and surface roughness needs to be more deeply investigated, and surface roughness should be embedded in the modeling of SKs to pick up the overall reflection patterns.

There have been endeavors to understand the role of roughness on rarefied gas transport, but the emphasis has been predominantly on larger-scale structures (i.e.,

^{*}Contact author: yichong.chen@ed.ac.uk[†]Contact author: livio.gibelli@ed.ac.uk

meso- or microscale) [41,42]. When examining gas-scattering dynamics, investigations should also consider nanoscale irregularities [23], which are brought by the height variation of wall atoms on the scale of a few nanometers. Current studies at the nanoscale [23,33,35,43–45] have favored simple geometrical constructions, such as surfaces with sinusoidal and triangular roughness, which typically have led to qualitative rather than quantitative analyses, thus limiting their wider applicability.

In the present paper, we propose a SK that quantitatively characterizes the influence of nanoscale roughness on the scattering dynamics. The proposed kernel is a linear combination of the Cercignani-Lampis (CL) model [4] for a smooth, thermal wall and the fully diffuse Maxwell model [1] for a highly rough surface. We find that the weighting coefficient of these two limiting conditions is elegantly described using a form of the Debye-Waller factor (DWF), which can be obtained experimentally and provides additional insights into the effects of surface roughness on the ACs. To assess the proposed SK, high-fidelity molecular dynamics (MD) simulations are performed for gas molecules interacting with various rough surfaces. The scattering reflection patterns are then measured accurately based on the deterministic gas molecular trajectories.

The remaining paper is organized as follows: Sections II and III provide a background of the SK theory and the spectral characterization of random roughness, respectively. Building on an established analogy between wave-surface scattering and GSIs, it allows us to propose the new SK in Sec. IV. Section V details the setup of our high-fidelity MD simulations with the implementation of random roughness that are carried out for both scattering and heat and flow measurements. In Sec. VI, we validate the scattering dynamics predicted by our SK on surfaces with different roughness characteristics, demonstrate its accuracy on Fourier and Poiseuille flow in large nanochannels and show how it provides better agreement than current ones with our benchmark MD simulations. Finally, concluding remarks are given in Sec. VII.

II. SCATTERING KERNELS AND THEIR ACCOMMODATION COEFFICIENTS

The scattering kernel, denoted as $\mathcal{R}(\xi' \rightarrow \xi; \mathbf{r}, t; \epsilon, \tau)$, provides the probability density of a gas molecule hitting the surface at a given location $\mathbf{r} - \epsilon$ and time $t - \tau$, with a velocity range of $[\xi', \xi' + d\xi']$, and subsequently rebounding from the surface at location \mathbf{r} and time t , within a velocity range of $[\xi, \xi + d\xi]$, where ϵ symbolizes the displacement and τ indicates the residence time [6]. The equation that relates the incident $f(\xi', \mathbf{r} - \epsilon, t - \tau)$ and reflected $f(\xi, \mathbf{r}, t)$ distribution functions can be obtained through a mass balance at the surface [6], leading to

$$\xi_n f(\xi, \mathbf{r}, t) = \int_{-\infty}^{\infty} d\epsilon \int_0^{\infty} d\tau \int_{\xi'_n < 0} \times |\xi'_n| \mathcal{R}(\xi' \rightarrow \xi; \mathbf{r} - \epsilon, t - \tau) d\xi', \quad (1)$$

where $\xi_n = \xi \cdot \mathbf{n}$ with \mathbf{n} being the unit vector normal to the surface pointing into the gas phase. The displacement and effective residence time during the scattering process

are typically small compared to the mean free path and characteristic time of the gas molecules undergoing collisions in the bulk region (i.e., the scattering is practically local and instantaneous), and the SK simplifies to $\mathcal{R}(\xi' \rightarrow \xi)$. This simplification is generally used and met in many situations of practical importance, including scattering from tight porous surfaces [35].

SKs satisfy the basic properties of (a) positiveness, (b) normalization, and (c) reciprocity [6,46]. Cercignani [6] proved that the simplest mathematical expression satisfying these properties takes the general form

$$\mathcal{R}_G(\xi' \rightarrow \xi) = \mathcal{R}_{G,t}(\xi' \rightarrow \xi_t) \mathcal{R}_{G,n}(\xi'_n \rightarrow \xi_n), \quad \text{where} \quad (2a)$$

$$\mathcal{R}_{G,t}(\xi' \rightarrow \xi_t) = \frac{(1 - q^2)^{-1}}{2\pi RT_w} \exp \left\{ -\frac{1}{1 - q^2} \frac{(\xi_t - q\xi'_t)^2}{2RT_w} \right\}, \quad (2b)$$

$$\mathcal{R}_{G,n}(\xi'_n \rightarrow \xi_n) = \frac{(1 - p)^{-1} \xi_n}{RT_w} \exp \left\{ -\frac{\xi_n^2 + p\xi_n'^2}{2RT_w(1 - p)} \right\} \times I_0 \left(\frac{\sqrt{p} \xi_n \xi'_n}{1 - p RT_w} \right), \quad (2c)$$

where ξ_t is the two-dimensional vector residing on the tangential plane with velocity components ξ_{t_1} and ξ_{t_2} , which possess equivalent scattering dynamics on an isotropic surface; $R = k_B/m$ is the specific gas constant, denoting the ratio between the Boltzmann constant k_B and the molecular mass of the gas m ; T_w denotes the wall temperature, and I_0 is the modified Bessel function of the first kind with zeroth order.

The bounded parameters $q \in [-1, 1]$ and $p \in [0, 1]$ are related to the ACs, expressing the tendency of the gas property associated with a specified function of molecular velocity $\varphi(\xi)$ to accommodate to the state of the wall. The general ACs are defined as [6,14,47]

$$\alpha(\varphi) = \frac{\int_{\xi'_n < 0} \varphi(\xi') |\xi'_n| f(\xi') d\xi' - \int_{\xi_n > 0} \varphi(\xi) |\xi_n| f(\xi) d\xi}{\int_{\xi'_n < 0} \varphi(\xi') |\xi'_n| f(\xi') d\xi' - \int_{\xi_n > 0} \varphi(\xi) |\xi_n| f_w(\xi) d\xi}, \quad (3)$$

where $f_w(\xi)$ is the nondrifting wall Maxwellian distribution. By setting $\varphi(\xi)$ as momentum and energy, one obtains ACs of common interest, such as $\alpha_t(\xi_{t_1})$ and $\alpha_t(\xi_{t_2})$ for the two components of tangential momentum (TMAC), $\alpha_{E_n}(\xi_n^2/2)$ for normal kinetic energy (NEAC), and $\alpha_E(\xi^2)$ for kinetic energy (EAC). Note that beam ACs $\alpha^b(\varphi)$ [14] are also used that become functions of the incident velocity and correspond to the cases of monoenergetic beams, $f(\xi') = \delta(\xi' - \xi_b)$ with ξ_b denoting a specified velocity.

It is noteworthy that the general definition of Eq. (3) possesses inherent limitations when employed for a parametric characterization of the SK. $\alpha(\varphi)$ proves to be dependent on the distribution function of impinging molecules [6,14]. Additionally, when the system approaches an equilibrium state, i.e., $f(\xi') \approx f(\xi) \approx f_w(\xi)$, both the numerator and denominator in Eq. (3) veer towards zero and computational inaccuracies arises. In this study, we have considered flows in the linear regime, where the averaged reflected quantity has a linear relationship with the corresponding averaged incident quantity. Consequently, as discussed in detail in Ref. [48], the ACs can

be determined by a linear regression analysis applied to the scattering data,

$$\alpha(\varphi) = 1 - \frac{\sum_i (\varphi'_i - \langle \varphi' \rangle) (\varphi_i - \langle \varphi \rangle)}{\sum_i (\varphi'_i - \langle \varphi' \rangle)^2}, \quad (4)$$

where $\langle \cdot \rangle$ denotes the mean and the index i ranges over the scattering data. It is worth mentioning that Eq. (4) can be derived from the general expression of ACs under the assumption of small deviations from equilibrium (i.e., linearized flows), as explained by Kuščer [14] and Cercignani [6], and that in this condition the ACs do not depend on the incident distribution function, thus having a more objective physical meaning.

All existing SKs can be readily obtained from the general form of Eq. (2) or through linear combinations of this form with weighting coefficients summing to unity. For elementary diffuse and specular reflections, as well as the CL model, the substitution of ACs into the general form follows

$$\text{Diffuse: } q = p = 0; \quad (5a)$$

$$\text{Specular: } q = p = 1; \quad (5b)$$

$$\text{CL: } q = 1 - \alpha_t, \quad p = 1 - \alpha_{E_n}. \quad (5c)$$

The Maxwell model, as a combination of elementary SKs, assumes that a fraction of incident gas molecules, determined by either TMAC or EAC, are re-emitted diffusely, while the remaining are specularly reflected. Despite its widespread application, this model oversimplifies the underlying scattering mechanism by employing only a single free parameter and falls short in reproducing the lobular re-emission patterns typically observed in molecular experimental studies [4], such as when a nearly monoenergetic atomic beam strikes a surface.

It is worth stressing that the CL model has also been obtained using alternative approaches that incorporate substantial physical interpretations [3,5,49–51]. Standing as a more comprehensive SK (with two explicitly defined ACs) than the Maxwell model, the CL model can be derived by solving the half-space transport equation that details the gas dynamics within the wall modelled as a homogeneous and nonpolar medium [3,5,51]. This transport equation includes a Fokker-Planck-type term characterizing the effect of the thermal motion of wall atoms, in essence, gas-phonon collisions [19,20,52]. In addition, a collision term of linear Boltzmann type can be effectively utilized for modeling the background medium of the wall.

III. SPECTRAL CHARACTERIZATION OF RANDOM ROUGH SURFACES

The fully diffuse and CL models cover the extremes of very rough and smooth (thermal) surfaces [6,15], respectively. However, few SKs systematically study roughness at the nanoscale, which lies between these two extremes. To develop a SK model that manages this intermediary range of roughness, we first present the methodology for characterizing surface roughness in this section.

Surface roughness is quantitatively described by its height, denoted as $h(\mathbf{x})$, with respect to position \mathbf{x} . The variation in height is captured by the correlation function $C(\mathbf{x}_2 - \mathbf{x}_1)$ evaluated between two separated points. Employing a Fourier

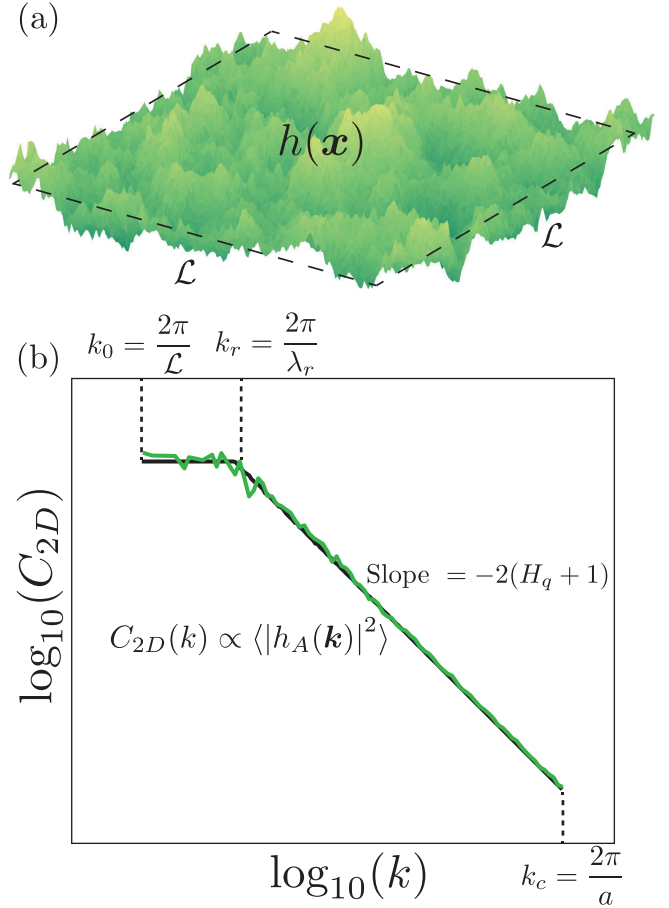


FIG. 1. (a) An example of a surface profile $h(\mathbf{x})$ with random roughness on a square plane. (b) A typical surface roughness power spectrum associated with the height profile $h(\mathbf{x})$, possessing a mean of zero and characterized, on average, by a second moment as defined by the height spectrum. The green line indicates the exact power spectrum taken from the sample in (a). Further details regarding the notations, e.g., Hurst exponent H_q , roll-off wavelength λ_r , and wave vector k_r , are common in the literature, such as in Ref. [53].

transform on this function and invoking the convolution theorem enables surface roughness analysis within the spatial frequency domain, characterized by wave vectors \mathbf{k} . This approach yields the surface power spectrum $C(\mathbf{k})$, also referred to as the power spectral density, which statistically describes the roughness by revealing the amplitude of height variations and the distribution of spatial frequencies \mathbf{k} —the inverse of the wavelength. Surfaces exhibiting large height variations over short length scales thus will show elevated spatial frequencies in their power spectra compared to smoother surfaces, making the power spectrum a useful tool to characterize surface roughness over diverse length scales.

If the surface statistical properties are isotropic and translationally invariant, then the dependency of the spectrum on the wave vector reduces to the magnitude, i.e., $C(\mathbf{k}) = C(k)$. For simplicity, while satisfying general validity, in this work we restrict our consideration to a square area $A = L^2$, as shown in Fig. 1(a). A two-dimensional spectrum $C_{2D}(k)$ thus can be expressed as [53]

$$C_{2D}(k) = \frac{(2\pi)^2}{A} \langle |\hat{h}_A(\mathbf{k})|^2 \rangle, \quad (6)$$

where the angle brackets stem from the spatial autocorrelation of height functions and denote ensemble averaging, while

$$\hat{h}_A(\mathbf{k}) = \frac{1}{(2\pi)^2} \int_A d^2x h(x) e^{-i\mathbf{k}\cdot\mathbf{x}} \quad (7)$$

is the Fourier transform of the zero-mean height profile $h(x)$, measured over the sample of area A . Note that, as shown in Fig. 1(b), there will be an upper and a lower limit to the wave vector within the spectrum. The largest feasible wave vector will be of order $2\pi/a$, where a embodies a short wavelength cutoff associated with the lattice constant. Conversely, the smallest feasible wave vector is of order $2\pi/L$, with L being the length dimension of the surface. Finally, it is worth stressing that the typical power spectrum shown in Fig. 1(b) can be observed in the fluidic channel fabrication of microchips, where the roughness of silicon wafer surfaces is found to be random and multiscale [53–56].

IV. GAS-SURFACE SCATTERING INSPIRED BY THE DEBYE-WALLER FACTOR

The investigation of GSIs could gain profound insights from the analogy with established wave-surface scattering [57], as exemplified in a study involving the scattering of electromagnetic waves by a randomly rough surface [49].

In the wave-surface scattering scenario, it is known that the wave vector of an incoming wave is altered by the thermal motion of the wall atoms as well as their nanostructure morphology, e.g., surface roughness. Indeed, experimentally recording both the incoming and outgoing wave vectors of x rays or neutrons serves as a useful method to elucidate the properties of the surface.

For the scenario of GSIs, the aforementioned analogy can be applied to a group of gas particles impinging the surface, whose incoming wave vectors get an imprint of the surface wave vectors on their reflection [58–61]. To be precise, a “gas wave vector” $\mathbf{k}_g = 2\pi/\lambda = m\xi/\hbar$ is defined via the de Broglie wavelength λ , and \hbar is the reduced Planck constant. The term “surface wave vectors” is used from here onward as an effective representation of wave vectors in the power spectrum $C_{2D}(k)$, stemming from the height profile after the Fourier transform (see Sec. III).

A. Debye-Waller factor for thermal motion

When a beam of gas particles scatters from rigid surfaces comprised of frozen atoms, the scattering is purely elastic, i.e., it does not involve energy transfer with the wall atoms. All scattered particles are found in perfectly sharp (delta function) peaks [62,63]—either a specular reflection on the perfectly smooth surface, such as that shown schematically in Fig. 2(a), or diffracted beams arising from the corrugated surface. The thermal motion of solid atoms attenuates this elastic scattering by a DWF [64] and leads to the spread of the scattered particles, as shown in Fig. 2(b). The DWF is defined as [15,61–63]

$$\text{DWF} = \exp[-\langle(\mathbf{u} \cdot \Delta\mathbf{k}_g)^2\rangle], \quad (8)$$

where \mathbf{u} is the displacement of the wall atom from its equilibrium position due to its thermal motion, $\Delta\mathbf{k}_g$ is the change

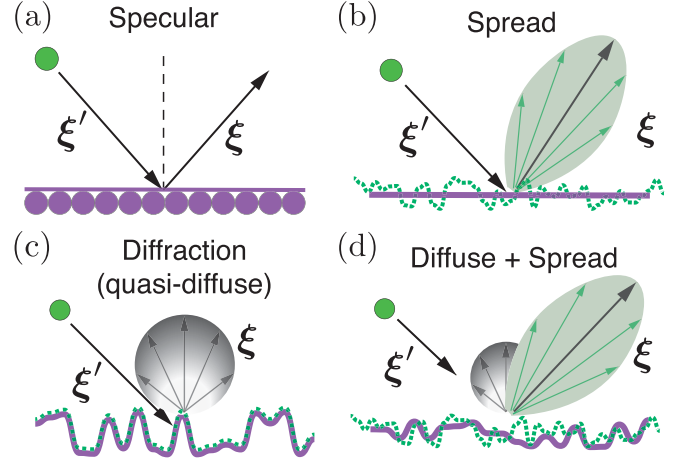


FIG. 2. Schematic illustrating gas molecule scattering patterns: (a) elastic specular reflection on a perfectly smooth rigid or frozen surface, (b) inelastic spread reflection on a perfectly smooth surface but which contains thermal motion, (c) diffraction-induced reflection on a rough surface, and (d) representative inelastic reflection factoring in both surface roughness and thermal motion on surfaces of interest in this work (i.e., containing nanoscale roughness).

of wave vector after scattering, and angle brackets denote the thermal averaging at a given temperature [15,62].

The DWF, alongside its complement, $1 - \text{DWF}$, hence provides approximate fractions of elastic and inelastic scattering events, respectively. Furthermore, the DWF exhibits temperature dependence, indicated as $\ln(\text{DWF}) \propto -T_w$ [61,62,65]. Consequently, it is not unexpected that in GSIs, the form of DWF noticeably coheres with the effects of wall temperature T_w on the ACs, characterized by an exponentially decaying relationship [66,67]. While the DWF has been shown to qualitatively describe the scattering physics related to thermal motion, it has not been explicitly used in the modeling of a SK.

B. Pseudo-Debye-Waller factor for rough surfaces

In this study, we have incorporated a DWF-inspired concept to account for the influence of surface roughness on scattering events. This adaptation stems from the fact that thermal motion causes wall atoms to deviate from their equilibrium positions, akin to the generation of a rough surface arising from a perfectly smooth plane. Here the roughness refers to a contour governed by the static potential energy surface (PES), beyond which the movement of a gas molecule is inhibited. Notably, these hard gas-surface collisions align closely with the physical model described by Cercignani [5,6] (see Sec. II), who, however, disregarded the roughness and presumed a perfectly flat PES, where gas molecules are specularly reflected.

We propose a pseudo Debye-Waller factor (PDWF) as follows:

$$\text{PDWF} \sim \exp[-\langle(\hat{h}_A(\mathbf{k}) \cdot \mathbf{k})^2\rangle], \quad (9)$$

in which the surface height $\hat{h}_A(\mathbf{k})$ bears an analogous relation to the thermal displacement \mathbf{u} . The change of wave vector $\Delta\mathbf{k}_g$ in Eq. (8), resulting as an imprint of the wall on the scattered

gas molecules, is replaced by the PES wave vector \mathbf{k} . This substitution conceptually indicates that alterations of gas wave vectors are directly proportional to the static surface wave vectors [57–59,68], which provides the basis for modeling of gas scattering on a rough surface.

Inspired by the expression of the DWF for harmonic potentials among wall atoms [15,69], the PDWF for roughness may be given as

$$\text{PDWF} = \exp \left[- \int_{k_{\min}}^{k_{\max}} k^2 C_{2D}(k) dk / \kappa^2 \right], \quad (10)$$

where κ is a fitting constant (see Sec. VIB) and serves as the characteristic wave vector for quantifying roughness intensity. The wave nature of the surface spectrum, as outlined in Sec. III, hence lends us a convenient and accurate method to compute the PDWF in Eq. (10) and which can now be incorporated into a SK that models roughness.

C. A new scattering model, incorporating surface roughness

We present a new scattering model that accounts for the effects of random surface roughness at standard or elevated temperatures, where quantum mechanical features are suppressed and classical scattering description applies [15,61,63,68,70]. For simplicity, we omit the atomic-rough corrugations of the PES that arise from the crystal lattice structure. These corrugations are often imperceptible within the range of the largest feasible wave vectors k_c , given their characteristic length scale can be even smaller than the cutoff wavelength a .

Classical molecular scattering may be dominated by two types of interactions or collisions. The first category stems from the thermal motion of solid atoms, perceived as weak perturbations owing to the fluctuating surface potential. These interactions are denoted as gas-phonon collisions in scattering studies [19,20,22,23,25–27], leading to a spread or lobular pattern (not necessarily surrounding the specular line of reflection) of the re-emitted particles [see Fig. 2(b)]. The second category encompasses hard gas collisions with a static PES. Substantial specular reflection is expected if the PES perceived by incident molecules is smooth on the scale of the de Broglie wavelength [15,63,68]. However, when considering very rough random surfaces, the re-emitted molecules are more likely to display a diffuse pattern, as shown in Fig. 2(c), which arises from the elastically diffracted beams occurring across the surface (at different points). These two types of scattering dynamics coexist for practical surfaces that involve nanoscale roughness, as illustrated in Fig. 2(d).

Our SK therefore accounts for a linear combination of these weak and hard collisions. Specifically, this includes the CL model, denoted as $\mathcal{R}_{\text{CL},t}$, considered to provide the most accurate description of molecular interactions with a smooth surface in thermal equilibrium, and the fully diffuse Maxwell model, \mathcal{R}_d , which characterizes hard collisions on random rough surfaces

$$\mathcal{R}_{\text{new},t} = B_1 \mathcal{R}_{\text{CL},t}(\alpha_{t,0}) + (1 - B_1) \mathcal{R}_d, \quad (11a)$$

$$\mathcal{R}_{\text{new},n} = B_2 \mathcal{R}_{\text{CL},n}(\alpha_{E_n,0}) + (1 - B_2) \mathcal{R}_d, \quad (11b)$$

where

$$B_1 = \text{PDWF}, \quad B_2 = C_n(\text{PDWF} - 1) + 1, \quad (11c)$$

in which $\alpha_{t,0}$ and $\alpha_{E_n,0}$ are the intrinsic magnitude of TMAC and NEAC for gas molecules on a thermal surface excluding roughness. These coefficients can be sourced either from beam experiments [15,62] conducted in low vacuum systems, provided the surface can be manufactured perfectly smooth, or by using MD simulations as done in this work.

In Eq. (11), the function B_1 signifies the fraction of molecules striking the surface without considerable alteration in their tangential velocity. This can be naturally related to the PDWF introduced in Sec. IV B. Note that $B_1 = \text{PDWF} = 1$ corresponds to a very smooth surface in thermal equilibrium. Its counterpart, $1 - B_1$, represents the fraction undergoing diffuse reflection, which relates the surface roughness intensity to the changes in tangential scattering dynamics. Unlike Maxwell’s conception that diffusely re-emitted gas is linked to the depth of the “stratum” [1], we found that both B_1 and $1 - B_1$ are, in fact, insensitive to penetration depth within the wall (see Appendix A); gas-scattering dynamics are consistent across any stratum, provided the roughness characterization remains similar at each level.

The function B_2 bears a similar meaning to B_1 , albeit for the normal velocity component. It necessitates independent treatment because, unlike momentum, the energy accommodation to the state of the surface, describing the normal scattering dynamics, is recognized to be slower [6,13,35]. Regarding the evaluation of B_2 , it can be postulated that either a straightforward fitting function or the simplest direct proportionality relationship, as indicated by the fitting constant $C_n \in [0, 1]$ in Eq. (11c), may exist in correlation with the PDWF.

The general TMAC and NEAC of the proposed SK readily follow

$$\alpha_t = B_1 \alpha_{t,0} + (1 - B_1), \quad (12a)$$

$$\alpha_{E_n} = B_2 \alpha_{E_n,0} + (1 - B_2). \quad (12b)$$

V. MODELLING THE SCATTERING USING MOLECULAR DYNAMICS

This study employs the MD method to simulate the scattering dynamics of gas molecules, using the open-source LAMMPS software [71]. In our system, gas molecules are modelled as monatomic for simplicity. Chemically active or very heavy gas molecules, such as oxygen and xenon, are intentionally excluded from our MD setup. These molecules, due to their strong intermolecular potentials with wall atoms, may “permanently” adsorb onto the surface, thus violating the assumption of negligible residence time.

The wall atoms are arranged in a face-centered cubic (FCC) configuration with a lattice parameter of 3.92 Å. Each wall is bounded by an outer edge of rigid wall atoms, inhibiting any wall movement, thereby maintaining the integrity of the defined system. Surface roughness is defined by imposing a power spectrum that maps directly onto crystal lattice coordinates, establishing a one-to-one correspondence between

TABLE I. Interatomic Lennard-Jones potential parameters (σ , ϵ) used in the MD simulations. Molecular masses m [u]: Ar = 39.948, He = 4.0026, Pt = 195.084, Au = 196.967.

Helium-gold [72]			Argon-platinum [48]		
Atom pairs	σ (Å)	ϵ/k_B (K)	Atom pairs	σ (Å)	ϵ/k_B (K)
He-He	2.64	10.890	Ar-Ar	3.405	119.80
Au-Au	2.630	2662.1	Pt-Pt	2.471	8053.6
He-Au	4.342	9.1355	Ar-Pt	2.940	79.139

spectrum values and lattice locations to generate the desired roughness pattern. Moreover, periodic boundary conditions are implemented in the nonconfined dimensions, with the roughness features seamlessly connected from one edge of the simulation box to the other. This consistent and connected roughness landscape ensures uniform GSIs across the entire simulation domain.

Two distinct groups of gas-surface combinations have been considered [helium-gold (He-Au) and argon-platinum (Ar-Pt)], with each combination investigated under various rough surface power spectra. The interatomic interactions were modelled using the standard 12-6 Lennard-Jones (LJ) potential, with parameters listed in Table I and a cutoff distance of $r_c = 15$ Å. The velocity-Verlet algorithm with a time step of 1 fs was utilized to integrate molecular trajectories.

Each MD simulation run consists of two parts: equilibration and production. During equilibration, a Nosé-Hoover thermostat maintains both gas molecules and wall atoms at a constant temperature, with a 100-fs time constant in the NVT ensemble. Two temperatures, 300 K and 600 K, are adopted, representing typical room temperature conditions of MEMS and NEMS devices and a test of scattering dynamics at elevated temperatures, respectively. Following equilibration, the thermostat on the gas molecules is deactivated to prevent any bias in their scattering dynamics, and gas-gas interactions are disabled, ensuring GSIs remain unaffected by the presence of possible gas adsorbed layers. The production run yields extensive Lagrangian data, from which scattering information of interest can be extracted. A virtual plane shown in Fig. 3, positioned at $r_c + h_{\max}$ parallel to the plane of the average

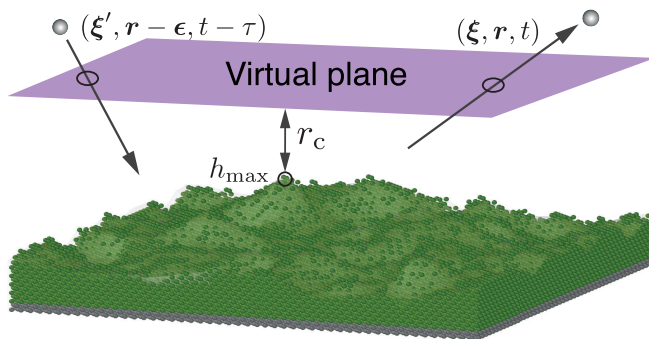


FIG. 3. Schematic of the scattering dynamics of gas molecules near a rough FCC wall. Scattering information for incident (e.g., $\xi', r - \epsilon, t - \tau$) and reflected (e.g., ξ, r, t) molecules is recorded at the virtual plane.

coordinates of the first layer of wall atoms, is used to flag atoms as they enter and exit the near-wall region, thereby defining the scattering events. Here h_{\max} represents the maximum height of the surface roughness. The inclusion of h_{\max} extends the near-wall region to include the influence of every wall atom. This extension does not affect the scattering dynamics since gas-gas interactions are disabled. Further details of this technique for recording scattering dynamics can be found in our previous works [13,35].

VI. RESULTS AND DISCUSSION

In this section, we first verify the expected features of surface roughness in our MD studies, elaborating on the computation of the PDWF from the PES measurement (Sec. VI A). Following this, we calibrate the constants within the proposed SK to best align with TMACs and NEACs across varying roughness intensities (Sec. VI B). We demonstrate that the proposed SK accurately predicts scattering dynamics under different test conditions (Sec. VI C). Finally, comparing macroscopic quantities derived from SK outcomes with those produced by rough explicit walls further demonstrates the better prediction of our proposed model over other existing SKs (Sec. VI D).

A. Surface roughness in MD and the corresponding computation of the PDWF

We start by presenting a sample rough surface generated within our MD setup using the surface power spectrum method, which provides the coordinates of the interfacial wall atoms, as shown in Fig. 4(a). Subsequently, Fig. 4(b) displays the corresponding PES measurement for this rough surface. In our study, the potential energy experienced by a molecule is mapped onto a grid and calculated as an ensemble average during the MD production run. The PES is then measured as a contour level where the potential energy is zero, $U(\mathbf{r}) = 0$, which, according to standard LJ potentials, signifies coordinates approximately one molecular diameter (σ) away from the wall atoms' center of mass. On comparison, Figs. 4(a) and 4(b) exhibit a close resemblance with an expected shift of σ in the normal direction. After adjusting their coordinate origins to a zero mean, we perform a radial average on the calculated discrete Fourier transform of both surface topographies in Figs. 4(a) and 4(b) to derive their power spectra, as shown in Fig. 4(c). The similarities between the input and PES-derived spectra, despite some minor differences near the crystal structure dimension a , show that our measured PES resembles quite well the atom-defined roughness. In our computation of the PDWF, which is a wave-vector-weighted moment of the spectrum formulated by Eq. (10), we use the measured PES because it reflects the actual irregularities felt by gas molecules. However, the results in Fig. 4 indicate that the error would be small had the PDWF been calculated using the roughness arising from the surface-atom positions. This approach of using PES wave vectors, determined when the molecule is near the bottom of the potential well, also follows the methodologies proposed by Beeby [58,59] and Goodman [60] for evaluating classical DWF.

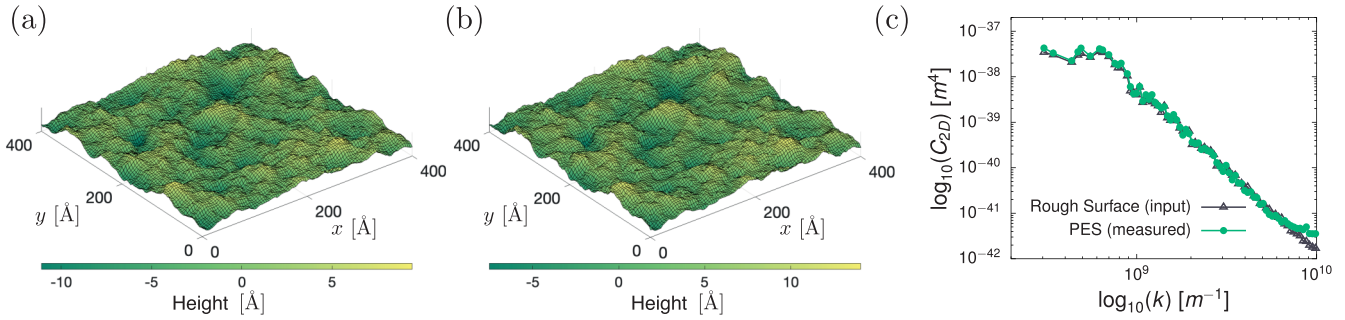


FIG. 4. (a) Coordinates of a sample random rough surface, with a root mean square (rms) of 3 Å and Hurst exponent $H_q = 0.8$; (b) PES measurement corresponding to the rough surface, obtained from the MD simulation of He-Au system at an equilibrium temperature of 300 K; (c) comparison of the two power spectra measured from the atom surface coordinates of panel (a) and the PES coordinates [defined at $U(\mathbf{r}) = 0$] of panel (b).

B. Calibration of scattering model

The proposed SK hinges on two sets of parameters, $\{\alpha_{r,0}, \alpha_{E_n,0}\}$, which feature the scattering dynamics from a thermal, smooth surface, and $\{\kappa, C_n\}$, which account for the surface roughness effects. The first two parameters are obtained by evaluating TMAC and NEAC from MD simulations on a thermal smooth FCC surface without any defects at the periodic boundaries, while the remaining two parameters are calibrated by fitting Eqs. (12) and (10) with the TMAC and NEAC values corresponding to various intensity of surface roughness, also determined by MD simulations. These ACs are presented in Fig. 5 for the sample cases of He-Au and Ar-Pt systems at two distinct temperatures (solid symbols), where the x error bars indicate the discrepancy between the

PDWF given by the input and measured spectra. It can be observed that the errors in the Ar-Pt system are more pronounced, attributable to its smaller GSI molecular diameter σ . This smaller diameter leads to increased corrugation of PES near the wall lattice structure, resulting in more significant discrepancies. Linear fitting curves were applied to the measured PES spectra points [based on Eq. (10) where κ is the fitting constant] for the tangential component, revealing a satisfactory agreement across different temperatures and systems. A summary of all parameters extracted from these MD simulations is listed in Table II for further reference.

Two remarks are worth making regarding the results reported in Fig. 5. First, the slope of NEAC is consistently smaller than that of TMAC, regardless of the temperature and

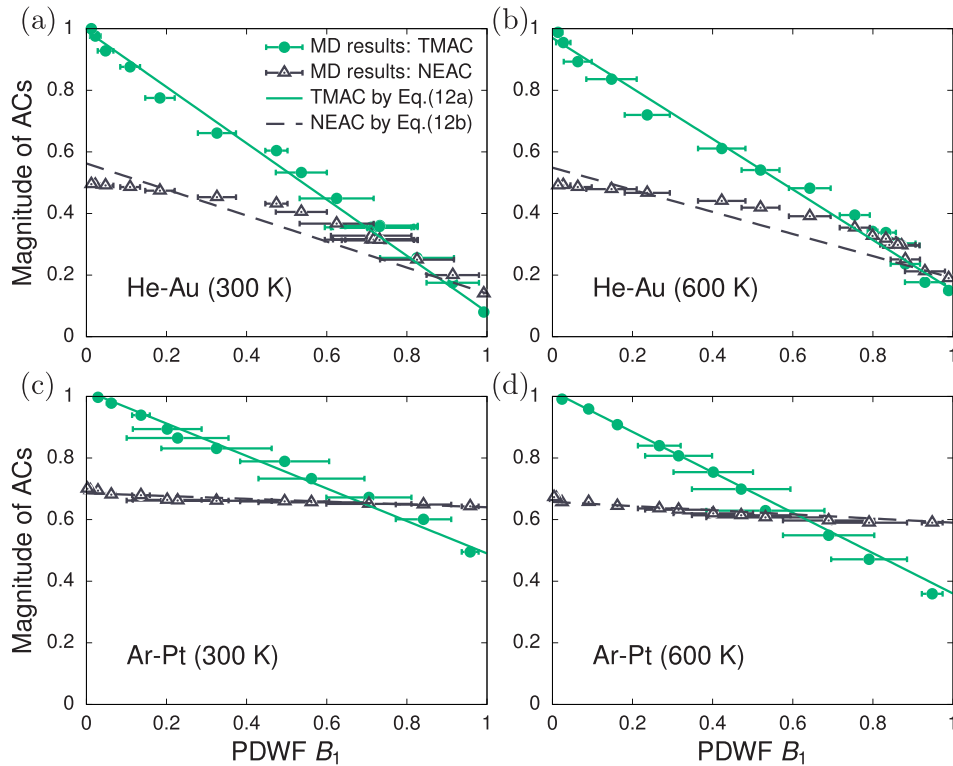


FIG. 5. Variation of the general accommodation coefficients with PDWF given by MD results for the He-Au system at (a) 300 K and (b) 600 K and the Ar-Pt system at (c) 300 K and (d) 600 K.

TABLE II. Reference values for the intrinsic accommodation coefficients ($\alpha_{t,0}$, $\alpha_{E_n,0}$) and the calibrated constants (κ , C_n).

T_w (K)	$\alpha_{t,0}$		$\alpha_{E_n,0}$		κ		C_n	
	300	600	300	600	300	600	300	600
He-Au	0.08	0.15	0.14	0.19	5.31×10^{-06}	5.43×10^{-06}	0.47	0.44
Ar-Pt	0.49	0.36	0.64	0.59	5.03×10^{-06}	5.24×10^{-06}	0.09	0.11

gas-surface combination. This highlights the slower accommodation of energy compared to momentum and indicates a lower influence of roughness on the normal component, thereby necessitating the introduction of the parameter C_n in Eq. (11). Second, unlike the constant κ that seems to

universally fit all data sets for the tangential component, the parameter C_n does not, and is dependent on the gas-surface combinations.

C. Scattering dynamics on rough surfaces at constant PDWF

In this section, we assess the scattering dynamics and investigate the role of the PDWF in our proposed SK model. Diverse rough surface spectra are first constructed, corresponding to the same PDWF value of 0.7, as shown by the five cases (four random rough surfaces, denoted as cases A–D, and one sinusoidal rough surface) in Fig. 6(a). Gas molecules re-emitted from these surfaces with varied roughness but the same PDWF should, in principle, exhibit similar scattering dynamics. In these simulations, the tangential and normal scattering components are treated as decoupled, dividing

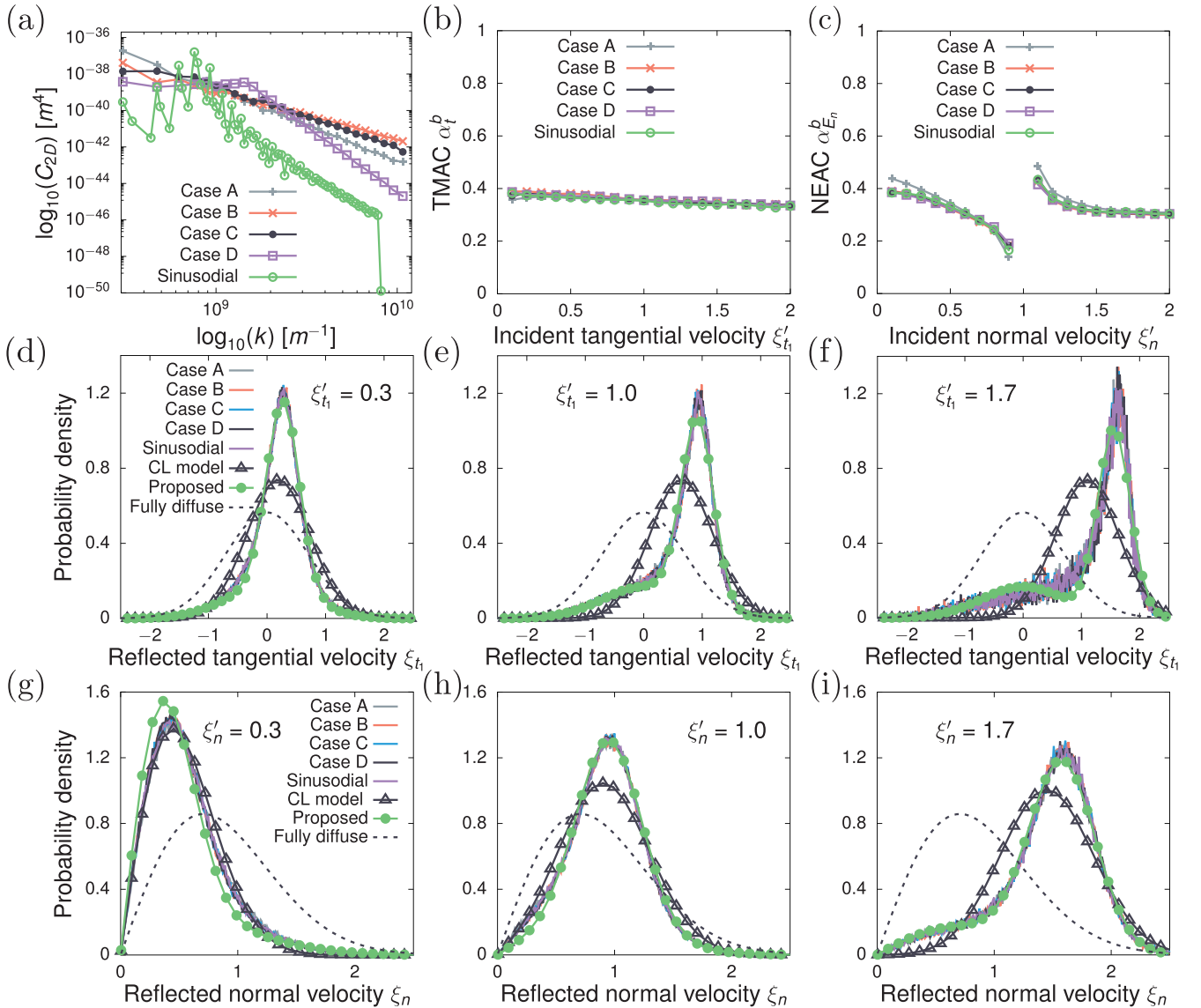


FIG. 6. (a) Rough surfaces chosen with different spectra but having the same PDWF = 0.7. The impact of the roughness of the chosen surfaces on scattering dynamics is shown through (b) beam TMACs, and (c) beam NEACs from the He-Au system at an equilibrium temperature of 300 K; comparison of the reflected velocity distribution for the [(d)–(f)] tangential and [(g)–(i)] normal velocities for monoenergetic beams predicted by MD and all scattering models. Velocities of the beams are normalized by the most probable speed $\sqrt{2RT}$.

incident molecules into distinct monoenergetic beams. This is achieved by selecting molecules whose tangential (or normal) velocity components are within the range of $[\xi', \xi' + \Delta\xi']$. Subsequently, the beam ACs and the re-emission probabilities of the velocity components within each range are determined. These numerical MD results are then compared with the theoretical predictions given by the proposed SK. In addition, for a more comprehensive analysis, comparisons are also made with SKs available in the existing literature.

Figures 6(b) and 6(c) provide a comparison between the beam TMAC and NEAC measurements. It is apparent that the magnitude and velocity dependence of these ACs align quite closely. While beam ACs may largely depend on the impinging velocity [8], this dependence is very weak in the systems simulated in this work. Hence, we employ general ACs for predicting scattering patterns for simplicity. Finally, numerical artifacts in the normal component are observed around the most probable speed in Fig. 6(c), as also noted by Yamamoto *et al.* [8] and Spijker *et al.* [48].

Figures 6(d)–6(f) present a comparison between the tangential scattering patterns of monoenergetic beams and those predicted by various SKs, including the fully diffuse, the CL, and our proposed model. Representative incident velocities, ξ'_n , are set at 0.3, 1.0, and 1.7. As can be seen, the scattering patterns obtained from surfaces with diverse spectra but identical PDWFs show considerable similarity, reinforcing the idea that PDWF is the key metric governing scattering on rough surfaces. It is evident that surfaces with different PDWFs will result in varying ACs, as seen in Fig. 5. Moreover, our proposed SK model best captures all the MD scattering patterns, incorporating two fractions representing the CL model (associated with weak perturbations) and the fully diffuse model (associated with hard collisions). However, when applied independently, neither the CL nor the fully diffuse model can well capture these patterns.

In the normal direction, as shown in Figs. 6(g)–6(i), our scattering model continues to offer the best agreement with the MD data, notwithstanding a minor deviation at the incident velocity $\xi'_n = 0.3$, attributed to our utilization of general ACs. However, such discrepancies are expected to have a negligible impact on macroscopic quantities, given the small weighting of gas molecules at this incident velocity.

Numerical scattering experiments were also conducted under various temperature conditions and gas-surface combinations. Similar qualitative trends were observed across all the systems studied, the details of which are presented in Appendix B.

D. Validation of the new SK under heat and flow

The final aspect of validating the proposed SK model involves assessing the accuracy of macroscopic flow profiles across a parallel channel. Here MD results from explicit physical walls will serve as the benchmark for comparison. Two problems are considered separately: (a) the force-driven Poiseuille flow and (b) the Fourier flow problem. In the Poiseuille flow scenario, an external force is applied to each gas atom in the streamwise direction, with the magnitude maintained small enough to keep the flow within the linear regime. The Fourier flow problem, on the other hand, in-

volves only applying a temperature change across the channel, allowing for an examination of how scattering dynamics influence temperature jumps at the walls.

For the MD benchmark simulations with explicit walls, gas-gas interactions are switched off, indicating that the flow systems are at an infinite Knudsen number ($\text{Kn} \rightarrow \infty$). This setup confirms that the influence on gas flow is solely due to GSIs. All SK models, including fully diffuse, Maxwell, CL, and our proposed model, were implemented in LAMMPS. In these MD simulations, the explicit atomic walls are replaced with stochastic walls, where the SK models determine the reflection behavior of incoming gas molecules, and the omission of wall atoms significantly reduces computational demands. It is important to emphasize that within kinetic theory, SKs are implemented at virtual planes, the sites of scattering measurements. The distance between these planes defines the effective channel height H , which is chosen to be sufficiently large to prevent confinement effects [73–76]. Due to code limitations within LAMMPS, we had to maintain gas-gas interactions in the stochastic wall simulations. However, we ensured that the lateral dimensions of the system were sufficiently large to effectively maintain a high Knudsen number.

Figure 7(a) presents normalized velocity profiles of gas flow within channels formed by different rough walls but under the same PDWF = 0.7, i.e., cases A–D and sinusoidal. For different cases considered, the velocity profiles within the effective channel H remain flat and in agreement with each other, consolidating the exclusive impact of scattering dynamics on velocity slip. In Fig. 7(b), we show the average of velocity profiles obtained from our MD simulations using explicit physical walls and compare it with those using SK stochastic walls. While the comparison reveals that a very small curvature exists in the velocity profile, caused by the Knudsen number not being truly infinite, there are significant discrepancies between the results of the different SKs. Our proposed SK gives a better agreement with the benchmark MD results.

Figures 7(c) and 7(d) show results similar to those in Figs. 7(a) and 7(b), albeit for the Fourier flow problem. As expected, in Fig. 7(c), the temperature profiles and temperature jumps given by the MD simulations of physical walls are similar. Notably, Fig. 7(d) reveals that both the CL model and the proposed model provide close predictions to the benchmark MD simulations than the other SKs. This closer agreement between CL and the proposed model may be attributed to the characteristics of the Fourier flow problem, particularly its relative insensitivity to the tangential scattering component, which is more affected by roughness.

VII. CONCLUDING REMARKS

In this work, we investigated the impact of nanoscale roughness on gas-surface scattering. Existing SKs do not contain enough information of the surface roughness features, and the quantitative relationship between the ACs, the gas-scattering patterns and the roughness remain unclear. To address this, we have proposed a SK, as a simple linear combination of the CL and Maxwell fully diffuse models. This combination is grounded in the rationale that the CL

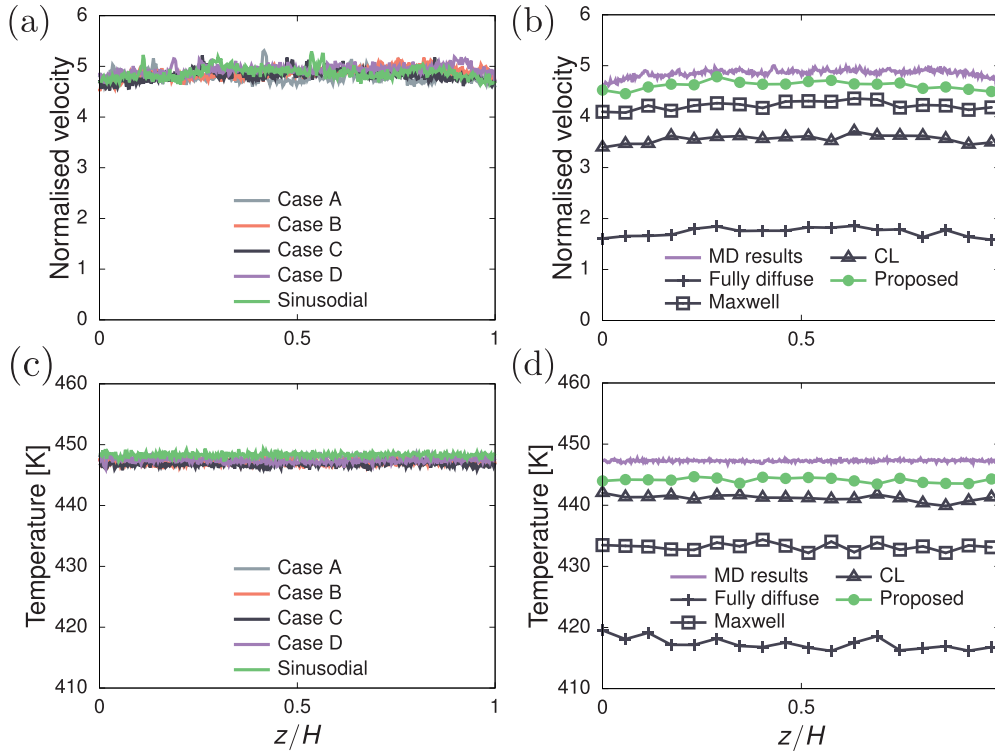


FIG. 7. Comparison of normalized velocity profiles for Poiseuille gas flow in the He-Au system at 300 K: (a) From MD simulations with explicitly constructed wall atoms and deactivated gas-gas interactions ($Kn \rightarrow \infty$), where $z/H \in [0, 1]$ indicates the region between virtual planes; and (b) from MD simulations employing stochastic walls, i.e., SKs, with active gas-gas interactions ($Kn \approx 461$). Temperature profiles for a Fourier flow problem: (c) Explicitly constructed wall atoms (bottom wall set at 600 K and top wall at 300 K) and (d) stochastic walls.

term accurately describes the gas-scattering dynamics on a thermal, smooth surface (dominated by weak perturbations from gas-phonon collisions), while the Maxwell fully diffuse term captures the hard collisions resulting from the irregularities of rough surfaces. We found that the weighting coefficient between the two models is elegantly described by a proposed PDWF, inspired by an analogy that roughness can be seen as waves superimposed on flat planes. The PDWF was evaluated via the power spectrum of the static PES, which can be easily obtained by MD simulations or experiments. The accuracy of various SKs were assessed using high-fidelity MD simulations, demonstrating that the proposed SK delivers the best agreement with the benchmark MD simulations

across the range of tested systems with varied roughness, temperature, and gas-surface combinations.

All MD files and post-processing scripts for the scattering data used in this work can be found in Ref.[77].

ACKNOWLEDGMENTS

This research was supported in the UK by the Engineering and Physical Sciences Research Council (EPSRC) under Grant No. EP/V012002/1. All MD simulations were run on ARCHER2, the UK’s national supercomputing service, funded by an EPSRC/ARCHER2 Pioneer Project.

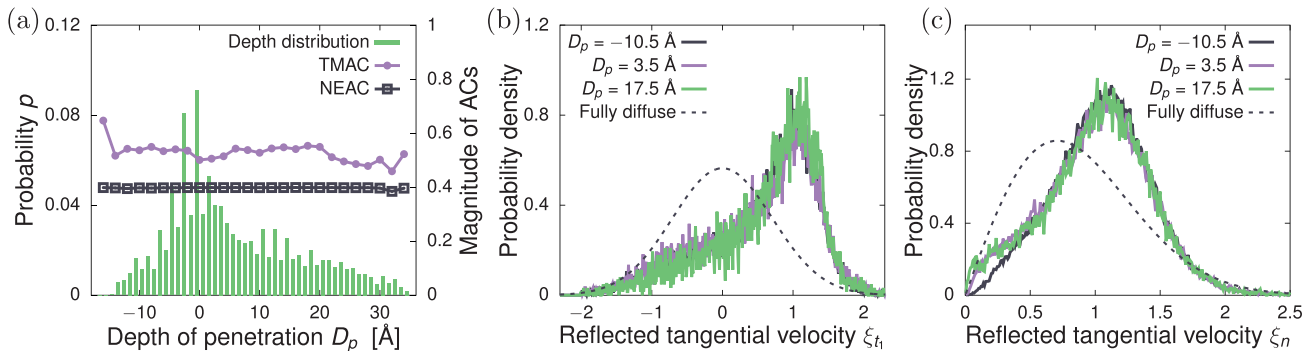


FIG. 8. (a) Depth of penetration distribution for gas molecules on a rough surface with $rms = 10 \text{ \AA}$ and $H_q = 1.0$ ($PDWF \approx 0.54$). Re-emission probability distribution for a monoenergetic molecular beam, with example cases of (b) tangential impinging velocity $\xi_{t1}' = 1.3$ and (c) normal impinging velocity $\xi_{n1}' = 1.3$.

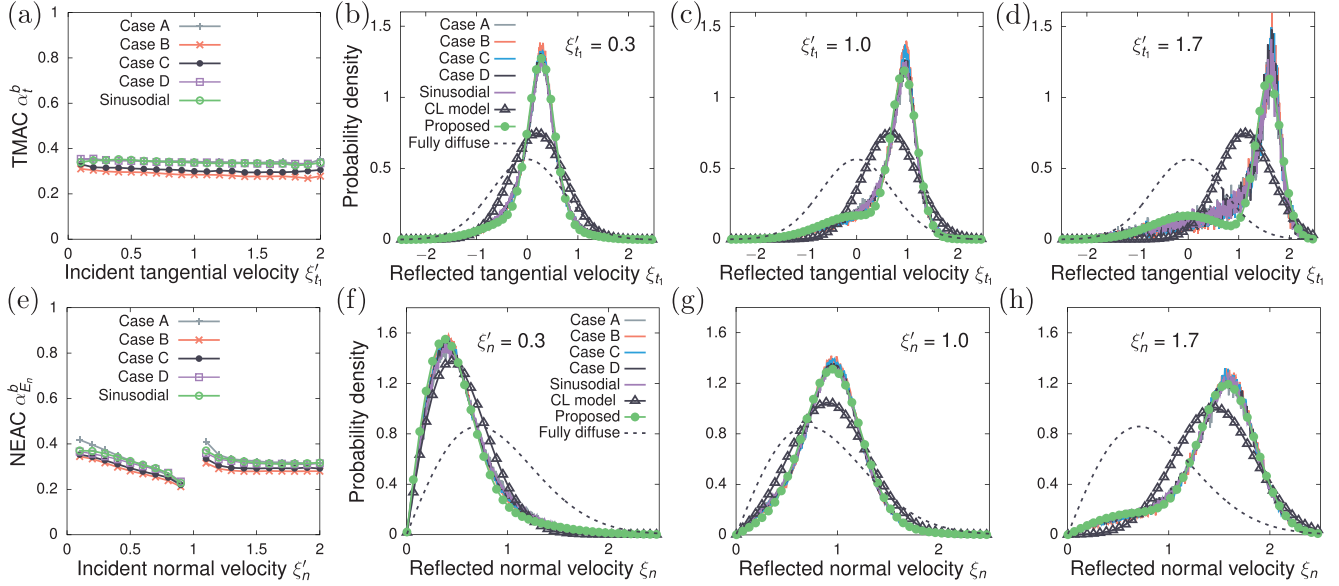


FIG. 9. (a) Beam TMACs and [(b)–(d)] tangential reflected velocity distributions for representative monoenergetic beams in the He-Au system are displayed, all at an equilibrium surface temperature of 600 K, and are predicted by existing scattering models and explicit MD, under surface roughness spectra with diverse characteristics yet maintaining a consistent magnitude of DWF = 0.7. (e) Beam NEACs and [(f)–(h)] normal reflected velocity distributions are derived from the aforementioned MD systems. Velocities of the beams are normalized by the most probable speed $\sqrt{2RT}$.

APPENDIX A: SCATTERING DYNAMICS AT DIFFERENT PENETRATION DEPTHS WITHIN THE WALL

Figures 8(a)–8(c) demonstrate consistent scattering dynamics independent of stratum depth. This is showcased both via the ACs [Fig. 8(a)] and the gas re-emission probability density distributions for tangential and normal components

[Figs. 8(b) and 8(c)], which convey more detailed information of the scattering patterns at different depths. Notably, the tangential scattering patterns are asymmetric, diverging from the symmetry intrinsic to the CL and fully diffuse reflection models, suggesting the coexistence of different collision patterns in GSIs.

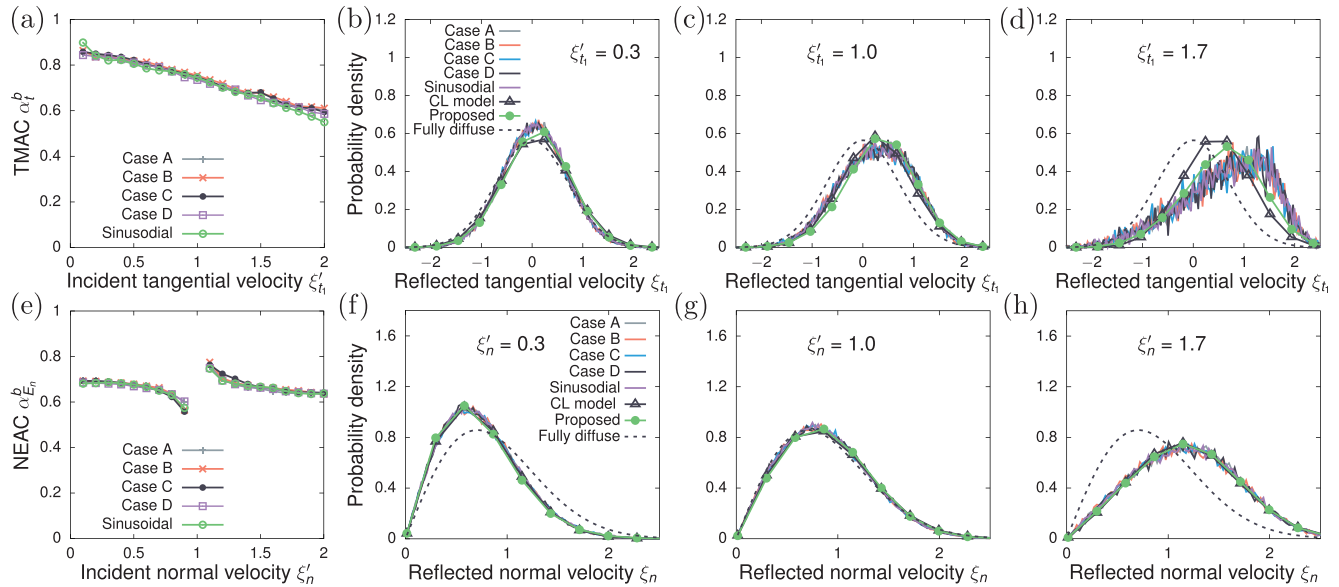


FIG. 10. (a) Beam TMACs and [(b)–(d)] tangential reflected velocity distributions for representative monoenergetic beams in the Ar-Pt system are displayed, all at an equilibrium surface temperature of 300 K, and are predicted by existing scattering models and explicit MD, under surface roughness spectra with diverse characteristics yet maintaining a consistent magnitude of DWF = 0.7. (e) Beam NEACs and [(f)–(h)] normal reflected velocity distributions are derived from the aforementioned MD systems. Velocities of the beams are normalized by the most probable speed $\sqrt{2RT}$.

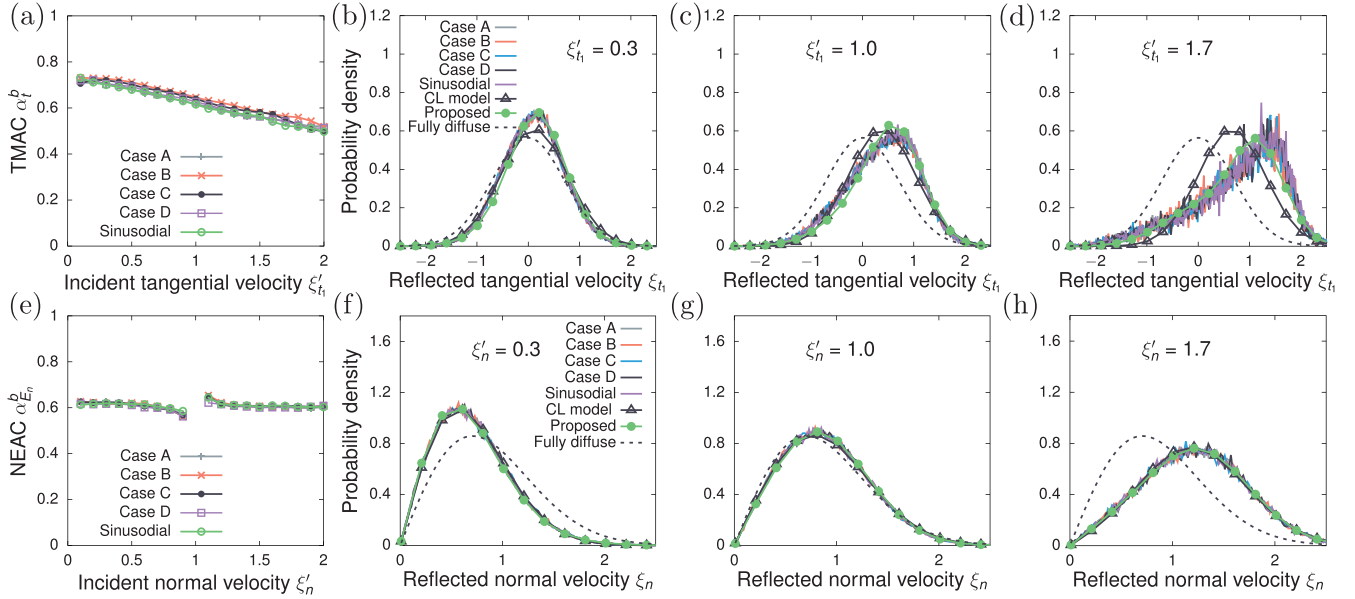


FIG. 11. (a) Beam TMACs and [(b)–(d)] tangential reflected velocity distributions for representative monoenergetic beams in the Ar-Pt system are displayed, all at an equilibrium surface temperature of 600 K, and are predicted by existing scattering models and explicit MD, under surface roughness spectra with diverse characteristics yet maintaining a consistent magnitude of $\text{DWF} = 0.7$. (e) Beam NEACs and [(f)–(h)] normal reflected velocity distributions are derived from the aforementioned MD systems. Velocities of the beams are normalized by the most probable speed $\sqrt{2RT}$.

APPENDIX B: COMPARISON OF SCATTERING DYNAMICS AT DIFFERENT EQUILIBRIUM TEMPERATURES AND GAS-SURFACE COMBINATIONS

Figures 9–11 show the scattering dynamics for the He-Au system at 600 K and Ar-Pt system at 300 K and 600 K, respectively. Simulations are conducted on the same surfaces as described in Sec. VIC, i.e., cases A–D and one sinusoidal rough surface with diverse spectra but the same PDWF = 0.7. For these results, three remarks are worth stressing. First, the temperature is insignificant on the roughness larger than the lattice structure, as further supported by the similar slope of general TMACs in Fig. 5. The temperature primarily affects the scattering dynamics through gas-phonon collisions,

encapsulated by the framework of the CL model. Second, the Ar-Pt system displays a more evident velocity-dependence behavior compared to He-Au, especially concerning the tangential velocity components. Yet one may reasonably expect that this dependence has minimal impact on the transport of low speed flows, provided the general ACs are accurately calibrated. Third, the performance of our proposed model decrease in the context of the Ar-Pt system. Although appearing smooth, the Ar-Pt system still displays minor PES corrugations due to small σ , leading to the so-called classical rainbow scattering [15,61,63]; the resulting effects can be incorporated, albeit introducing additional complexity to the proposed SK model.

- [1] J. C. Maxwell, VII. On stresses in rarefied gases arising from inequalities of temperature, *Philos. Trans. R. Soc.* **170**, 231 (1879).
- [2] M. Epstein, A model of the wall boundary condition in kinetic theory., *AIAA J.* **5**, 1797 (1967).
- [3] I. Kuščer, J. Mozina, and F. Krizamič, in *Rarefied Gas Dynamics, Proceedings of the Seventh International Symposium*, edited by S. N. Dino Dini and C. Cercignani (Edizioni Tecnico Scientifica, Pisa, 1971), p. 97.
- [4] C. Cercignani and M. Lampis, Kinetic models for gas-surface interactions, *Transp. Theory Stat. Phys.* **1**, 101 (1971).
- [5] C. Cercignani, Scattering kernels for gas-surface interactions, *Transp. Theory Stat. Phys.* **2**, 27 (1972).
- [6] C. Cercignani, *The Boltzmann Equation and Its Applications* (Springer, Berlin, 1988).
- [7] R. G. Lord, Some extensions to the Cercignani–Lampis gas-surface scattering kernel, *Phys. Fluids A* **3**, 706 (1991).
- [8] K. Yamamoto, H. Takeuchi, and T. Hyakutake, Scattering properties and scattering kernel based on the molecular dynamics analysis of gas-wall interaction, *Phys. Fluids* **19**, 087102 (2007).
- [9] H. Struchtrup, Maxwell boundary condition and velocity dependent accommodation coefficient, *Phys. Fluids* **25**, 112001 (2013).
- [10] L. Wu and H. Struchtrup, Assessment and development of the gas kinetic boundary condition for the Boltzmann equation, *J. Fluid Mech.* **823**, 511 (2017).
- [11] R. D. Brancher, S. Stefanov, I. Graur, and A. Frezzotti, A kinetic model for gas adsorption-desorption at solid surfaces under non-equilibrium conditions, *Vacuum* **174**, 109166 (2020).

- [12] J. Deng, J. Zhang, T. Liang, J. Zhao, Z. Li, and D. Wen, A modified Cercignani–Lampis model with independent momentum and thermal accommodation coefficients for gas molecules scattering on surfaces, *Phys. Fluids* **34**, 107108 (2022).
- [13] Y. Chen, L. Gibelli, J. Li, and M. K. Borg, Impact of surface physisorption on gas scattering dynamics, *J. Fluid Mech.* **968**, A4 (2023).
- [14] I. Kuščer, Phenomenology of gas-surface accommodation, in *Rarefied Gas Dynamics, Proceedings of the Ninth International Symposium*, edited by M. Becker and M. Fiebig (DFVLR-Press, Porz-Wahn, Germany, 1974), pp. E.1–21.
- [15] F. O. Goodman and H. Y. Wachman, *Dynamics of Gas–Surface Scattering* (Academic Press, New York, 1976).
- [16] R. M. Logan and J. C. Keck, Classical theory for the interaction of gas atoms with solid surfaces, *J. Chem. Phys.* **49**, 860 (1968).
- [17] J. C. Tully, Washboard model of gas–surface scattering, *J. Chem. Phys.* **92**, 680 (1990).
- [18] T. Liang, Q. Li, and W. Ye, A physical-based gas–surface interaction model for rarefied gas flow simulation, *J. Comput. Phys.* **352**, 105 (2018).
- [19] V. D. Borman, S. Yu. Krylov, and A. V. Prosyranov, Theory of nonequilibrium phenomena at a gas–solid interface, *Zh. Eksp. Teor. Fiz.* **94**, 271 (1988) [*Sov. Phys. JETP* **67**, 2110 (1988)].
- [20] S. Y. Krylov, Molecular transport in sub-nano-scale systems, in *AIP Conference Proceedings* (American Institute of Physics, Washington, DC, 2003), Vol. 663, pp. 735–742.
- [21] A. Frezzotti and L. Gibelli, A kinetic model for fluid–wall interaction, *Proc. Inst. Mech. Eng. Part C* **222**, 787 (2008).
- [22] S. Brull, P. Charrier, and L. Mieussens, Gas-surface interaction and boundary conditions for the Boltzmann equation, *Kinet. Relat. Models* **7**, 219 (2014).
- [23] S. Brull, P. Charrier, and L. Mieussens, Nanoscale roughness effect on Maxwell-like boundary conditions for the Boltzmann equation, *Phys. Fluids* **28**, 082004 (2016).
- [24] K. Aoki, P. Charrier, and P. Degond, A hierarchy of models related to nanoflows and surface diffusion, *Kinet. Relat. Models* **4**, 53 (2011).
- [25] K. Aoki and V. Giovangigli, Kinetic model of adsorption on crystal surfaces, *Phys. Rev. E* **99**, 052137 (2019).
- [26] K. Aoki and V. Giovangigli, Kinetic theory of chemical reactions on crystal surfaces, *Physica A* **565**, 125573 (2021).
- [27] K. Aoki, V. Giovangigli, and S. Kosuge, Boundary conditions for the Boltzmann equation from gas-surface interaction kinetic models, *Phys. Rev. E* **106**, 035306 (2022).
- [28] L. J. Stacy, A determination by the constant deflection method of the value of the coefficient of slip for rough and for smooth surfaces in air, *Phys. Rev.* **21**, 239 (1923).
- [29] M. Seidl and E. Steinheil, Measurement of momentum accommodation coefficients on surfaces characterized by auger spectroscopy, sims and leed, in *Rarefied Gas Dynamics, Proceeding of the Ninth International Symposium*, edited by M. Becker and M. Fiebig (DFVLR-Press, Porz-Wahn, Germany, 1974), pp. E9.1–E9.12.
- [30] L. Thomas and R. Lord, Comparative measurements of tangential momentum and thermal accommodations on polished and on roughened steel spheres, in *Rarefied Gas Dynamics, Proceeding of the Eighth International Symposium*, edited by K. Karamcheti (Academic Press, New York, 1974), pp. 405–412.
- [31] D. Blanchard and P. Ligrani, Slip and accommodation coefficients from rarefaction and roughness in rotating microscale disk flows, *Phys. Fluids* **19**, 063602 (2007).
- [32] W. M. Trott, J. N. Castañeda, J. R. Torczynski, M. A. Gallis, and D. J. Rader, An experimental assembly for precise measurement of thermal accommodation coefficients, *Rev. Sci. Instrum.* **82**, 035120 (2011).
- [33] G. Arya, H.-C. Chang, and E. J. Maginn, Molecular simulations of Knudsen wall-slip: effect of wall morphology, *Mol. Simul.* **29**, 697 (2003).
- [34] M. Ozhgibesov, T. Leu, C. Cheng, and A. Utkin, Studies on argon collisions with smooth and rough tungsten surfaces, *J. Mol. Graphics Modell.* **45**, 45 (2013).
- [35] Y. Chen, J. Li, S. Datta, S. Y. Docherty, L. Gibelli, and M. K. Borg, Methane scattering on porous kerogen surfaces and its impact on mesopore transport in shale, *Fuel* **316**, 123259 (2022).
- [36] P. Perrier, M. Hadj-Nacer, J. G. Méolans, and I. Graur, Measurements and modeling of the gas flow in a microchannel: Influence of aspect ratios, surface nature, and roughnesses, *Microfluid. Nanofluidics* **23**, 97 (2019).
- [37] F. Sharipov, Application of the Cercignani–Lampis scattering kernel to calculations of rarefied gas flows. i. plane flow between two parallel plates, *Eur. J. Mech. B Fluids* **21**, 113 (2002).
- [38] T. Basdanis, G. Tatsios, and D. Valougeorgis, Gas–surface interaction in rarefied gas flows through long capillaries via the linearized Boltzmann equation with various boundary conditions, *Vacuum* **202**, 111152 (2022).
- [39] H. Yamaguchi, T. Hanawa, O. Yamamoto, Y. Matsuda, Y. Egami, and T. Niimi, Experimental measurement on tangential momentum accommodation coefficient in a single microtube, *Microfluid Nanofluid* **11**, 57 (2011).
- [40] F. Sharipov and M. R. Moldover, Energy accommodation coefficient extracted from acoustic resonator experiments, *J. Vac. Sci. Technol. A* **34**, 061604 (2016).
- [41] C. Zhang, Y. Chen, Z. Deng, and M. Shi, Role of rough surface topography on gas slip flow in microchannels, *Phys. Rev. E* **86**, 016319 (2012).
- [42] W. Su, H. Liu, Y. Zhang, and L. Wu, Rarefaction cloaking: Influence of the fractal rough surface in gas slider bearings, *Phys. Fluids* **29**, 102003 (2017).
- [43] H. Sun and M. Faghri, Effect of surface roughness on nitrogen flow in a microchannel using the direct simulation monte carlo method, *Numer. Heat Transfer, Part A* **43**, 1 (2003).
- [44] B.-Y. Cao, M. Chen, and Z.-Y. Guo, Effect of surface roughness on gas flow in microchannels by molecular dynamics simulation, *Int. J. Eng. Sci.* **44**, 927 (2006).
- [45] F. D. Sofos, T. E. Karakasidis, and A. Liakopoulos, Effects of wall roughness on flow in nanochannels, *Phys. Rev. E* **79**, 026305 (2009).
- [46] I. Kuščer, Reciprocity in scattering of gas molecules by surfaces, *Surf. Sci.* **25**, 225 (1971).
- [47] F. Sharipov and V. Seleznev, Data on internal rarefied gas flows, *J. Phys. Chem. Ref. Data* **27**, 657 (1998).
- [48] P. Spijker, A. J. Markvoort, S. V. Nedeá, and P. A. J. Hilbers, Computation of accommodation coefficients and the use of velocity correlation profiles in molecular dynamics simulations, *Phys. Rev. E* **81**, 011203 (2010).

- [49] M. Williams, A phenomenological study of gas-surface interactions, *J. Phys. D: Appl. Phys.* **4**, 1315 (1971).
- [50] T. Cowling, On the Cercignani–Lampis formula for gas–surface interactions, *J. Phys. D: Appl. Phys.* **7**, 781 (1974).
- [51] S. Takata, S. Akasobe, and M. Hattori, A revisit to the Cercignani–Lampis model: Langevin picture and its numerical simulation, in *Recent Advances in Kinetic Equations and Applications* (Springer, Berlin, 2021), pp. 345–365.
- [52] J. V. Barth, Transport of adsorbates at metal surfaces: From thermal migration to hot precursors, *Surf. Sci. Rep.* **40**, 75 (2000).
- [53] B. N. Persson, O. Albohr, U. Tartaglino, A. Volokitin, and E. Tosatti, On the nature of surface roughness with application to contact mechanics, sealing, rubber friction and adhesion, *J. Phys.: Condens. Matter* **17**, R1 (2005).
- [54] C. Bora, E. Flater, M. Street, J. Redmond, M. Starr, R. Carpick, and M. Plesha, Multiscale roughness and modeling of mems interfaces, *Tribol. Lett.* **19**, 37 (2005).
- [55] C. Gui, M. Elwenspoek, N. Tas, and J. G. Gardeniers, The effect of surface roughness on direct wafer bonding, *J. Appl. Phys.* **85**, 7448 (1999).
- [56] L. Székely and A. Guttman, New advances in microchip fabrication for electrochromatography, *Electrophoresis* **26**, 4590 (2005).
- [57] F. G. Bass and I. M. Fuks, *Wave Scattering from Statistically Rough Surfaces: International Series in Natural Philosophy* (Elsevier, Amsterdam, 2013), Vol. 93.
- [58] J. Beeby, The scattering of helium atoms from surfaces, *J. Phys. C: Solid State Phys.* **4**, L359 (1971).
- [59] J. Beeby, The scattering of atoms from surfaces: The one-phonon contribution, *J. Phys. C: Solid State Phys.* **5**, 3438 (1972).
- [60] F. O. Goodman, On the use of a Debye–Waller-type factor in gas–surface scattering theory, *Surf. Sci.* **65**, 37 (1977).
- [61] J. Manson and S. Miret-Artés, Atom–surface scattering in the classical multiphonon regime, *Phys. Chem. Chem. Phys.* **24**, 16942 (2022).
- [62] J. A. Barker and D. J. Auerbach, Gas–surface interactions and dynamics; Thermal energy atomic and molecular beam studies, *Surf. Sci. Rep.* **4**, 1 (1984).
- [63] G. D. Billing, *Dynamics of Molecule Surface Interaction* (John Wiley & Sons, New York, 2000).
- [64] M. A. Krivoglaz, *Teoriya Rasseyaniya Rentgenovskikh Lučei i Teplovyh Neitronov Real’nymi Kristallami* (Nauka, Moscow, 1967).
- [65] R. J. Glauber, Time-dependent displacement correlations and inelastic scattering by crystals, *Phys. Rev.* **98**, 1692 (1955).
- [66] D. Menzel and J. Kouptsidis, Energy transfer by single collisions and by trapping in thermal accommodation, in *Rarefied Gas Dynamics, Proceeding of the Ninth International Symposium*, edited by M. Becker and M. Fiebig (DFVLR-Press, Porz-Wahn, Germany, 1974), pp. E.14–1–11.
- [67] B.-Y. Cao, M. Chen, and Z.-Y. Guo, Temperature dependence of the tangential momentum accommodation coefficient for gases, *Appl. Phys. Lett.* **86**, 091905 (2005).
- [68] I. Kuščer, Phenomenological aspects of gas–surface interaction, in *Fundamental Problems in Statistical Mechanics IV*, edited by E. Cohen and W. Fiszdon (Ossolineum, Warsaw, 1978), pp. 441–467.
- [69] C. Kittel, *Introduction to Solid State Physics* (John Wiley & Sons, New York, 2005).
- [70] G. A. Bird, *Molecular Gas Dynamics and the Direct Simulation of Gas Flows* (Oxford University Press, Oxford, 1994).
- [71] S. Plimpton, Fast parallel algorithms for short-range molecular dynamics, *J. Comput. Phys.* **117**, 1 (1995).
- [72] M. Liao, R. Grenier, Q. To, M. de Lara-Castells, and C. Leonard, Helium and argon interactions with gold surfaces: Ab initio-assisted determination of the He–Au pairwise potential and its application to accommodation coefficient determination, *J. Phys. Chem. C* **122**, 14606 (2018).
- [73] Q. Sheng, L. Gibelli, J. Li, M. K. Borg, and Y. Zhang, Dense gas flow simulations in ultra-tight confinement, *Phys. Fluids* **32**, 092003 (2020).
- [74] C. Corral-Casas, J. Li, M. K. Borg, and L. Gibelli, Knudsen minimum disappearance in molecular-confined flows, *J. Fluid Mech.* **945**, A28 (2022).
- [75] C. Corral-Casas, Y. Chen, M. K. Borg, and L. Gibelli, Density and confinement effects on fluid velocity slip, *Phys. Rev. Fluids* **9**, 034201 (2024).
- [76] B. Shan, W. Su, L. Gibelli, and Y. Zhang, Molecular kinetic modelling of non-equilibrium transport of confined van der Waals fluids, *J. Fluid Mech.* **976**, A7 (2023).
- [77] Example LAMMPS MD input scripts can be downloaded from <https://doi.org/10.7488/ds/7747>.